Influence of the alkali-silica reaction on the mechanical degradation of concrete

Esposito, Rita; Anac, Caner; Hendriks, M.A.N.; Copuroglu, Oguzhan

DOI
10.1061/(ASCE)MT.1943-5533.0001486

Publication date
2016

Document Version
Accepted author manuscript

Published in
Journal of Materials in Civil Engineering

INFLUENCE OF THE ALKALI-SILICA REACTION ON THE MECHANICAL DEGRADATION OF CONCRETE

Rita Esposito, [1] Caner Anaç, [2] Max A.N. Hendriks, [3] [4] and Oğuzhan Çopuroğlu [5]

Abstract

The alkali-silica reaction (ASR) is an important problem that has yet to be completely understood. Due to the complexity of this phenomenon, a number of studies have been conducted to characterize its kinetics, its impact on the material and its structural consequences. This paper focuses on the deteriorating impact of ASR on concrete material, not only in terms of concrete swelling but also in consideration of the induced mechanical degradation. The relationships between concrete expansion and various engineering properties, which are key parameters in structural assessments, are investigated. First, new mechanical test results are presented. Second, available literature data on the evolution of engineering properties of ASR-affected concrete under free-expansion conditions, are collected and statistically analysed. The elastic modulus was found to be the best indicator for identifying the progression of ASR in concrete. Conversely, the evolution of compressive strength was observed to potentially mask damage resulting from the ASR. The tensile behaviour of affected concrete was better represented by the splitting tensile test.

Keywords: Alkali-silica reaction (ASR), Damage assessment, Degradation, Mechanical properties

INTRODUCTION

[1]Ph.D. Candidate, Dept. of Structural Engineering, Delft University of Technology, Stevinweg 1, 2628CN, Delft, The Netherlands. E-mail: r.esposito@tudelft.nl.

[2]Ph.D. Candidate, Dept. of Structural Engineering, Delft University of Technology, Stevinweg 1, 2628CN, Delft, The Netherlands. E-mail: c.anac@tudelft.nl.

[3]Associate professor, Dept. of Structural Engineering, Delft University of Technology, Stevinweg 1, 2628CN, Delft, The Netherlands. E-mail: m.a.n.hendriks@tudelft.nl.

[4]Professor, Dept. of Structural Engineering, Norwegian University of Sciences and Technology (NTNU), Richard Birkelands vei 1a, 7491, Trondheim, Norway.

[5]Assistant professor, Dept. of Structural Engineering, Delft University of Technology, Stevinweg 1, 2628CN, Delft, The Netherlands. E-mail: o.copuroglu@tudelft.nl.

Because the service life design of concrete structures has become an important topic in construction projects, considerations of durability issues are being included in the design phase. In this group, the alkali-silica reaction (ASR) is known for its complex chemistry and physical mechanisms, which makes predicting the behaviour of ASR-affected concrete structures very challenging.

Various investigations regarding the structural effects of the ASR have been conducted over the past decade. Attention has particularly been focussed on infrastructures such as hydroelectric power plants and bridges. The first studies were performed on dams and accompanied by structural analyses (Léger et al. 1996; Malla and Wieland 1999; Huang and Pietruszczak 1999; Ulm et al. 2000; Capra and Sellier 2003; Li and Coussy 2004; Saouma et al. 2007; Comi et al. 2009; Saouma 2013), along with the development of the first engineering models concerning ASR. Later, structural effects of the ASR on concrete members were investigated under laboratory conditions, primarily using shear and flexural tests on beams (Fan and Hanson 1998; Clayton et al. 1990; den Uijl 2002; Multon 2004; Inoue et al. 2012; Martin et al. 2012; Mikata et al. 2012; Miyagawa et al. 2012; Ramezanianpour and Hajighasemali 2012). Meanwhile, the framework was narrowed to investigate the anisotropic expansion behaviour induced by the coupling between expansive alkali-silicate gel, material expansion and external mechanical loading (Larive 1998; Multon 2004).

Various experimental campaigns also studied the degradation of mechanical properties induced by gel expansion in laboratory samples stored under free-expansion conditions (Swamy and Al-Asali 1988; Larive 1998; Ahmed et al. 2003; Monette 1997; Multon 2004; Ben Haha 2006; Giaccio et al. 2008; Sargolzahi et al. 2010; Giannini and Folliard 2012; Lindgård 2013; Sanchez et al. 2014) The experimental focus was on the compressive strength, which is the most widely used material parameter in structural assessments. The results were contradictory and a clear degradation trend for the compressive strength could not be identified. Conversely, the elastic modulus was always found to be sensitive to the reaction.

RESEARCH SIGNIFICANCE

By considering a wider scope of structural assessments, this paper aims to highlight the importance of mechanical degradation in relation to ASR-induced concrete expansion. In current practice, the ASR reactivity of a concrete mix is evaluated through accelerated laboratory tests on unconstrained samples. However, the results from these tests do not directly relate to the real performance of concrete within a structure. The performance of concrete is generally expressed in terms of expansion and expansion rates, which can considerably differ substantially for different concrete mixes and environmental conditions (Larive 1998; Lindgård 2013). Here the observed expansion and expansion rates were considered as given. The specific goal was to find a trend between the deterioration of the mechanical properties and the observed swelling of concrete under free-expansion conditions regardless of the wide variety of concrete mixes used and the experimental conditions applied.

First, the experimental results obtained by the authors are presented. The classification and normalisation procedures are described as an introduction to the following statistical analysis. Second, available literature data on the mechanical degradation of ASR-affected concrete under free-expansion conditions are summarised. The relation between ASR-induced expansion and the mechanical degradation of concrete is statistically analysed.

EXPERIMENTAL RESEARCH

In 2010 a large experimental campaign was begun at the Delft University of Technology (TU Delft) under the framework of the PAT-ASR project (Performance Assessment Tool for Alkali-Silica Reaction) (Anaç et al. 2012). The scope of this research was to investigate the damage effects induced by the ASR in concrete on various scales: from microscopic to macroscopic scale.

In this section, the results for the macroscopic scale on the deteriorating impact of ASR on concrete in terms of expansion and the degradation of mechanical properties are reported. The experimental results are evaluated in a statistical context through the introduction of a classification and a normalisation procedure. Each concrete mix is classified on the basis of the expansion value obtained in a in prescribed testing duration. Their mechanical properties are normalised to identify a degradation trend.

Materials and test methods

Two comparable concrete mixes were adopted throughout this study using Dutch and Norwegian aggregates. The latter represents the concrete mix used in the Nautesund bridge (Norway), which exhibited severe ASR damage. The Nautesund bridge is a unique case, because from construction to demolition, all materials and structural details were properly documented. Through a collaboration between the Delft University of Technology (TU Delft) and the Norwegian Roads Public Administration (NPRA), concrete samples of this structure were used in the PAT-ASR project for verification purposes.

Concrete mixes cast with Dutch and Norwegian aggregates are respectively classified as RR1 and RR2 mixes, as clarified in the next subsection. Norwegian aggregates in the RR2 mix were primarily composed of coarse-grained quartz, quartzite, gneiss, metarhyolite and other minor rock types. By implementing the point count method, it was estimated that 33% of aggregates with a size of 0-8 mm and 36% of coarse gravel were potentially alkali-reactive. Dutch aggregates in the RR1 mix were primarily composed of quartzite, quartz, (calcareous) chert, volcanic rock fragments and other minor rock types. Thus far no alkali reactivity has been reported for these aggregates. The adopted mix proportions of cement/fine aggregates/coarse aggregates/water were 1:2.93:1.68:0.46 for the RR1 mix and 1:3.03:1.74:0.45 for the RR2 mix by weight. NORCEM Industri (CEM I 42.5R) cement with a dosage of 380 $\mathrm{kg/m^3}$ and an equivalent $\mathrm{Na_2O_{eq}}$ content of 1.17% was used. The two concrete mixes were designed to have a similar aggregate gradation and a comparable 28-day compressive strength. Therefore, to properly define the mix design, the density, the apparent specific gravity (ASG), the water absorption and the moisture of aggregates were identified following ASTM C127 (2012a) and ASTM C128 (2012b). Tables 1 and 2 list the characteristics of the concrete mixes and cement, respectively.

Due to the large number of samples needed, they were cast in six sessions; in each session, control casting cubes, which were not subjected to ASR treatment, were prepared. Table 3 lists the concrete properties for each cast. Cube specimens with sides of 150 mm were stored for 28 days at 20 $^{\circ}\mathrm{C}$ in a fog room and subsequently tested under uniaxial compression loading following

NEN-EN 12390-3:2002 (2002). The load was applied at a constant rate of 0.60 MPa/s. In order to determine the evolution of the mechanical properties of ASR affected concrete, expansion and mechanical tests were performed on prisms and cubes stored at 38 °C and a relative humidity of greater than 96% (RILEM TC 219-ACS Alkali-Silica Reaction in Concrete Structures 2011). An overview of the storage conditions and sample sizes is given in Table 4. The samples were placed on top of a metallic grid in plastic boxes; 2 cm of water at the bottom of the box ensured high humidity. The plastic boxes were placed in custom plastic reactors containing water, in which the plastic boxes were immersed 10 cm in water. The reactors included built-in heating elements to heat the water. During the storage period temperature sensors were placed inside the boxes and in the reactors to control the temperature, whereas humidity sensors were installed only in the reactors. The samples were tested at 14, 28, 49, 91, 182, 252 and 365 days.

The expansion values were measured on 75x75x280-mm prisms according to the procedure proposed by RILEM recommendation AAR-3 (2011). Tests for for determining the static elastic modulus were performed on 100x100x400-mm prisms in agreement with ISO 1920-10:2010(E) (2010). Linear Variable Differential Transformers (LVDTs) were employed to measure vertical and horizontal displacements. The vertical LVDTs were centrally placed on each side of the sample over a length of 200 mm. The alternative method was selected, in which the strain and stress on the test specimen were continuously measured during the loading cycle. First, a basic stress of 0.50 MPa was applied for 60 s; afterwards, the strain was constantly increased until the peak was reached. The static elastic modulus E_{st} and the Poisson ratio ν were determined in the elastic phase of the curve, between the basic stress level and one third of the peak stress. The peak stress was chosen as a measure of the compressive strength f_{c}. The splitting tensile strength $f_{\mathrm{t,sp}}$ was measured for cubes with sides of 150 mm, which is in agreement with EN 13290-6:2009 (2009). The load was applied with a constant increase of 0.05 MPa/s.

Results

Table 5 lists the results from the expansion and the mechanical tests for both mixes. Each result was determined as the average of three measurements performed on samples of the same cast. The number of the cast from which each set of three samples was prepared is listed, thereby making a distinction between samples employed for the expansion and mechanical tests (e.g., 4 - 1 means that the expansion measurements were performed on samples prepared in cast number 4, while the corresponding mechanical tests refer to samples prepared in cast number 1). The mix design, the properties of fresh concrete and the 28-day cubic compressive strength of each cast are presented in Tables 1 and 3. The coefficients of variation of 28-day cubic compressive strength for the RR1 and RR2 concrete mixes were found to be 5.1 and 4.4%, respectively.

The asymptotic expansion obtained after one year was 0.11% for the RR1 mix and 0.18% for the RR2 mix (Figure 1(a)). Both mixes appeared reactive according to the RILEM recommendation AAR-0 (2012) and exceeded the recommendation expansion threshold values of 0.05 and 0.1%. The classification proposed by RILEM recommendation AAR-0 (2012) has been extended and further applied in the next section. Three classes of mixes were defined on the basis of the maximum concrete expansion reached within the testing time. The concrete mixes were classified as potentially reactive mixes (PR) if their expansion was $0.05\% \leq \varepsilon \leq 0.10\%$, or as reactive mixes (RR) if their expansion was $0.10\% < \varepsilon < 0.50\%$, or as extremely reactive mixes (ER) if their expansion was greater than 0.50%. If the concrete expansion was found to be $\varepsilon \leq 0.05\%$, the mix was considered to be non-reactive.

In Figure 1(b)-d, the degradation of the mechanical properties is reported in terms of normalised values versus expansion. Each normalised value β_P was obtained as the ratio between the current property value P and its reference one P^{ref}. The latter was estimated at a reference expansion of 0.05%, which is the value used to discriminate between non-reactive and potentially reactive concrete. This normalisation procedure is also adopted in the next section, in which available literature data are compared and analysed to describe the degradation behaviour.

The mechanical properties exhibited a slight increase during the first 90 days, followed by a degradation trend. The static elastic modulus (Figure 1(b)) of concrete mix RR1 exhibited minor variations and ranged between 99 and 107% of its reference value. Conversely, the concrete mix RR2 exhibited a maximum degradation of 35%. The normalised compressive strength (Figure

1(c)) exhibited a pronounced initial increase from 0.76 to 0.90 for RR1 concrete and from 0.88 to 0.97 for RR2 concrete. After both concrete mixes tend to the asymptotic value of 1. The splitting tensile strength (Figure 1(d)) reported a similar trend for both mixes. After a relatively small initial increment a degradation was observed, which obtained a maximum value of 23% for concrete mix RR1 and of 26% for concrete mix RR2.

In conclusion, the studied RR1 and RR2 mixes were both classified as reactive, which is in agreement with the proposed classification procedure. The RR2 concrete presented highest expansion, and it showed a relevant degradation in terms of its static elastic modulus and splitting tensile strength. The RR1 concrete, which presented lower expansion, showed a constant tendency for the static elastic modulus; however, its deterioration in terms of splitting tensile strength follows the same trend as that for the RR2 concrete. Both concrete mixes showed an initial increase in compressive strength, which was followed by a nearly constant progression when the reference value was approached.

STUDY OF THE MECHANICAL DEGRADATION INDUCED BY THE ALKALI-SILICA REACTION

To study the degradation of mechanical properties induced by the alkali-silica reaction, available literature experimental data were collected, along with the data presented in the previous section. A statistical analysis was performed to determine trends in the degradation behaviour.

Overview of literature data

Over the past 30 years, various authors have tested the degradation of mechanical properties induced by ASR in concrete samples stored under free-expansion conditions. In this overview the results obtained by Swamy et al. (1988), Larive (1998), Ahmed et al. (2003), Monette et al. (1997), Multon (2004), Ben Haha (2006), Giaccio et al. (2008), Sargolzahi et al. (2010), Giannini and Folliard (2012), Lindgård (2013) and Sanchez et al. (2014), as well as the results presented earlier in this paper are used.

Tables 6 and 7 list the concrete properties and storage conditions employed by the various authors. A variety of natural aggregates was used. In a few cases (Swamy and Ahmed) non-natural aggregates were adopted to accelerate the reaction. This practice, although often criticised, is still sometimes used to understand the ASR mechanism in concrete (Bažant et al. 2000). The water-to-cement ratio, W/C, chosen in these studies varied between 0.30 and 0.61, and the equivalent alkali content ranged between 0.40 and 2.25%. The majority of the authors stored their samples at 38 °C (± 2 °C), ensuring a high relative humidity or placing the samples in water. These storage conditions are now prescribed by current standards and recommendations (e.g., ASTM C1293 (2001) and RILEM recommendation AAR-3 (2011)). In general, the samples were not wrapped and stored in plastic or metal boxes. Pre-treatment was applied by 6 of 12 authors, who primarily kept the samples at 20 °C in fog room. The samples were demoulded after one day, with the exception of Larive, who kept the samples in moulds for three days.

To analyse the data, mixes were classified on the basis of the asymptotic expansion value obtained within the prescribed testing time (Table 8). If a test was terminated before the prescribed testing duration had elapsed (Monette and Giannini), the asymptotic expansion was chosen at the end of the test. In contrast, when the test went beyond the testing duration (Larive and Sargolzahi), the asymptotic expansion was calculated by interpolation. In the cases where different storage conditions were used (Ben Haha and Lindgård), the asymptotic expansion was defined for the condition closest to the one proposed by RILEM recommendation AAR-3 (2011). The classification procedure presented in the previous section was adopted, and the concrete mixes were divided into potentially reactive (PR, $0.05\% \leq \varepsilon \leq 0.10\%$), reactive (RR, $0.10\% < \varepsilon < 0.50\%$) and extremely reactive (ER, $\varepsilon \geq 0.50\%$). Non-reactive mixes ($\varepsilon \leq 0.05\%$) were not considered. To distinguish between the different data sets, the name of the first author was indicated. If the same authors tested more than one mix in the same reactivity class, an Arabic number was added to the data set name (e.g., Swamy-ER1 and Swamy-ER2). If an author tested the same mix with different proportions, a Roman numeral between i and iii was added to the data set name (e.g., Ben Haha-PR1ia, Ben Haha-PR1iia and Ben Haha-PR1iiia). If an author tested the same mix design under different storage conditions, the letters a, b and c were added to the data set name (e.g., Lindgård-PR1a, Lindgård-PR1b and Lindgård-PR1c). To compare the results, the normalisation procedure presented in the previous section was adopted. The reference values at an expansion of $\varepsilon = 0.05\%$ were generally interpolated and they are listed in Table 8.

The majority of the authors studied the degradation of the compressive strength f_{c} (10 of 12 authors) and of the static elastic modulus E_{st} (9 of 12 authors), as shown in Table 8. The tensile behaviour was studied by 7 of 12 authors, who preferred the use of the splitting tensile strength $f_{\mathrm{t,sp}}$ above the modulus of rupture MOR and the direct tensile strength $f_{\mathrm{t,dir}}$. Non-destructive tests for determining the dynamic elastic modulus E_{dyn} were chosen by 5 of 12 authors.

Figures 2 and 3 report the variations in the mechanical properties as functions of the concrete expansion. Four zones were defined: the low-expansion zone ($\varepsilon < 0.05\%$), the moderate-expansion zone ($0.05\% \leq \varepsilon \leq 0.10\%$), the high-expansion zone ($0.10\% < \varepsilon < 0.50\%$) and the extreme-expansion zone ($\varepsilon \geq 0.50\%$). Each data point is an average of the results obtained from testing three samples, with the exception of Swamy, who adopted two samples. For clarity, the figures employ a non-uniformly scaled expansion axis and the legend is reported in Table 8. Figures 4 and 5, which will be discussed in the next subsection, show the data with a uniformly scaled expansion axis.

It was found that the elastic modulus is subjected to a significant degradation (Figures 2(a) and 2(b)). Both the static and dynamic elastic moduli marginally increase for expansion values up to 0.03%. Subsequently, a slight degradation is observed in the low- and moderate-expansion zones; however their mean values remain close to unity in these zones. For expansion values greater than 0.10%, both of the stiffness properties decreased at similar rate. The maximum degradation was obtained in the extreme-expansion zone, with a reduction of 92% for the static elastic modulus and of 86% for the dynamic one. The non-destructive test provided a more dense data cluster with respect to the destructive test.

The compressive strength was extensively investigated by many authors, although Swamy and Al-Asali stated in 1988, *ipse dixit* "compressive strength is not a good indicator of the initiation or progress of ASR". Figure 2(c) confirms this tendency. In the low-expansion zone, the normalised value of compressive strength ranged between 0.59 and 1.62, with an average of 0.92. The data sets that obtained the lowest and highest normalised compressive strength values are the mixes PR1ia and PR2ia, respectively, (both tested by Ben Haha (2006)), which contained the lowest alkali content (Na_2O_{eq} = 0.4%) and were stored at a temperature of 20 °C under high humidity. Due to the low alkali content and the non-accelerated storage conditions, it can be hypothesised that the ASR did not lead to a significant concrete expansion and that the increase in strength can be attributed to the hydration process. Excluding these data sets, the maximum normalised value in the low-expansion zone equals 1.04. In the moderate-expansion zone, the data cluster narrows, and the normalised value of the compressive strength increases to 1.28. For expansion values greater than 0.15% the majority of the concrete mixes exhibit a degradation in term of strength; however, the data show a substantial number of exceptions. The maximum degradation is obtained in the extreme-expansion zone, with a reduction of 46%.

The tensile behaviour of ASR-affected concrete (Figure 3) was found to be sensitive to the test method, as previously observed for unaffected concrete. Whereas the splitting (Figure 3(a)) and flexural (Figure 3(b)) tests show an important decrease in the strength for high-expansion values, the direct tensile strength (Figure 3(c)) appears to be less sensitive. In the low-expansion zone, the normalised values of all three tensile strengths are close to unity. After the data clusters spread out, and both the splitting tensile strength and the modulus of rupture drastically decrease. The direct tensile strength exhibits a relevant degradation only in the extreme-expansion zone. However, the data are limited to only three concrete mixes tested by the same author (Ahmed et al. 2003), which are classified as reactive and extremely reactive. The few data points are spread over an expansion scale that ranges between -0.03 and 2.70%; therefore, a detailed picture of the degradation trend is missing, which can strongly influence the estimation of the reference values. The three strengths exhibit a maximum degradation in the extreme-expansion zone, with a reduction of 53% for the splitting tensile strength (Figure 3(a)), 89% for the modulus of rupture (Figure 3(b)), and 38% for the direct tensile strength (Figure 3(c)).

Statistical analysis

To determine the degradation behaviour of the mechanical properties induced by the alkali-silica reaction in free-expansion samples, a statistical analysis was performed. The normalised data were fitted on the basis of two formulations: an S-shaped curve and a piecewise linear curve. The four zones (low-, moderate-, high- and extreme-expansion zones) were considered to define the weights of each data point. Within each zone data points have the same weight, whereas the sum of the weights for each zone is equal within a weighted least squares fitting process. In this way a bias resulting from an unequal distribution of data points along the expansion axis is limited.

The S-shaped curve is a revised version of the degradation law proposed by Saouma and Perotti (2006) and expresses the normalised value of each property β_P as a function of the expansion ε, whereby four parameters are employed:

$$\beta_P = \frac{P}{P^{\mathrm{ref}}} = \beta_0 - (\beta_0 - \beta_\infty)\,\frac{1 - \exp\left(-\frac{\varepsilon}{\varepsilon_{\mathrm{c}}}\right)}{1 + \exp\left(-\frac{\varepsilon - \varepsilon_{\mathrm{l}}}{\varepsilon_{\mathrm{c}}}\right)} \tag{1}$$

where P and P^{ref} are the current and reference values of the chosen property, respectively; β_0 and β_∞ are the normalised property values at zero expansion and at the asymptotic expansion, respectively; and ε_{l} and ε_{c} are the latency and characteristic expansion values, respectively. The latency expansion ε_{l} defines the delay before a relevant degradation of the mechanical property is observed: the lower the latency expansion, the earlier the degradation is observed. The characteristic expansion ε_{c} contributes to the degradation rate, which is defined as the average decrease between ε_{l} and $\varepsilon_{\mathrm{l}} + 2\varepsilon_{\mathrm{c}}$.

Figure 4 shows the resulting S-shaped curves along with the experimental data. The fitting coefficients and the estimation errors, in terms of standard deviation, are reported in Table 9.

In Figure 4(a) the elastic modulus data are denoted by grey dots for destructive tests and by white dots for non-destructive tests. The fitting was formulated by considering all the data (thick continuous line) or by distinguishing between static (thick dash-dot line) and dynamic (thin continuous line) elastic modulus data. The curves exhibit a minor difference only in the extreme-expansion zone. Therefore, all the data can be considered to be representative of the stiffness degradation in concrete subjected to the ASR. The estimation error is 7%. The resulting latency time ε_1 is extremely small (on the order of 10^{-14}), which confirms the fast stiffness degradation starting in the low-expansion zone. The maximum, β_0, and the minimum, β_∞, normalised values of the elastic modulus equal 1.06 and 0.19.

Figure 4(b) shows the degradation S-shaped curve for the compressive strength. Due to the nature of the formulation, the initial increase in strength cannot be captured; as a result the maximum normalised value β_0 is equal to 1.00 and the latency expansion ε_1 is 0.51%. The S-shaped curve exhibits an asymptote at 0.64. The estimation error is 15%.

In Figure 4(c), the tensile strength data are denoted by grey, white and black dots to indicate the splitting, flexural and direct tensile tests, respectively. The fitting was formulated by considering all the data (thick continuous line) or by distinguishing between the three test methods. As previously mentioned, the test type has a strong influence on the resulting strength. Consequently, it is more appropriate to consider each test method separately. The curve based on the splitting tensile strength data (thick dash-dot line) provides the best fitting with an error of 8%. Its normalised value can range between 1.01 and 0.60. The degradation becomes pronounced after a latency expansion ε_1 of 0.35%. The modulus of rupture (thin continuous line) begins to degrade at approximately the same expansion level (ε_1 = 0.37%); it can reach a maximum deterioration of 76%. The estimation error is 20%, which is relatively high. The direct tensile strength (thin dash-dot line) exhibits a maximum degradation of 30%. The degradation starts at a latency expansion ε_1 of 2.15%, meaning that the fitting mainly follows the behaviour of the concrete mix Ahmed-ER2. The estimation error is 12%.

The statistical analysis was extended by considering a continuous piecewise linear function. This choice was made to allow for an increase in the mechanical properties, e.g., as observed for the compressive strength. The continuity points are represented by the expansion values that delimit the four zones; the formulation is as follows:

$$\beta_P = \frac{P}{P^{\mathrm{ref}}} = \begin{cases} q_{\mathrm{l}} + m_{\mathrm{l}}\varepsilon & \varepsilon \leq 0.05\% \\ q_{\mathrm{m}} + m_{\mathrm{m}}\varepsilon & 0.05\% < \varepsilon \leq 0.1\% \\ q_{\mathrm{h}} + m_{\mathrm{h}}\varepsilon & 0.1\% < \varepsilon \leq 0.5\% \\ q_{\mathrm{e}} + m_{\mathrm{e}}\varepsilon & \varepsilon > 0.5\% \end{cases} \tag{2}$$

where *q* and *m* the linear coefficients for each zone. Due to the continuity condition, the number of unknown coefficients reduces to five; three of the coefficients can be determined as follows:

$$q_{\mathrm{m}} = q_{\mathrm{l}} + (m_{\mathrm{l}} - m_{\mathrm{m}})\,0.05; \quad q_{\mathrm{h}} = q_{\mathrm{m}} + (m_{\mathrm{m}} - m_{\mathrm{h}})\,0.1; \quad q_{\mathrm{e}} = q_{\mathrm{h}} + (m_{\mathrm{h}} - m_{\mathrm{e}})\,0.5 \tag{3}$$

Figure 5 shows the resulting piecewise linear curve along with the experimental data. The fitting coefficients and the estimation errors, in terms of standard deviation, are reported in Table 9. The elastic modulus degradation (Figure 5(a)) was well described by the piecewise linear curve. The estimation error and the degradation rate, which were evaluated in the high-expansion zone, provide results that are similar to those obtained from the S-shaped curve fitting. For expansion values greater than 2.60% this formulation provides unrealistic negative normalised values for the elastic modulus; therefore, zero residual stiffness should be considered after this limit. The piecewise linear curve better described the behaviour of the compressive strength (Figure 5(b)), which shows an increase in the moderate-expansion zone. The total estimation error is slightly decreased to 13%. However, considering the moderate-expansion zone only, the estimation error is reduced from 20 to 13%. The piecewise linear curve exhibited similar trend and estimation error with respect to the S-shaped curve for the splitting tensile strength (Figure 5(c)). This formulation is able to capture the slight increase in strength observed for the modulus of rupture in the moderate-expansion zone.

In Figure 6(a), the best curve fitting results are presented along with an error band equal to 2σ. The piecewise linear curve was chosen to describe the compressive strength behaviour, whereas the S-shaped curve was chosen to describe the other properties. The tensile strength behaviour has been reported in terms of the splitting test results. Both static and dynamic elastic modulus data were considered for describing the stiffness degradation. According to the curve fitting studies, the elastic modulus was found to be the best indicator of ASR signs in concrete. The data show a relevant degradation, already at early expansion, which is characterized by the highest rate. For high-expansion values ($\varepsilon > 2.00\%$) the residual stiffness is 20% of the reference value. Conversely, the compressive strength behaviour is described with an initial gain of 15% and a maximum reduction of 46%. However, the estimation error is high, approximately 13%. The tensile behaviour appears to be well described by the splitting test results. In the high-expansion zone the tensile strength degrades at a similar rate as the elastic modulus, but its deterioration is delayed. The residual value is 46%.

Alternately, Figure 6(b) shows the differences in degradation behaviour from comparing the stiffness and strength properties. When the elastic modulus reaches 85% of its original value, both strengths decrease at a similar rate but still slower than the degradation rate of the elastic modulus. At a normalised value of $\beta_E = 0.50$ for the elastic modulus, the normalised splitting strength obtains an asymptotic value of $\beta_{f_{\mathrm{t,sp}}} = 0.60$. The compressive strength experiences a drastic deterioration to a normalised value of the elastic modulus of $\beta_E = 0.20$.

In engineering, it is common practice to express the stiffness E and tensile strength f_{t} of unaffected concrete as a function of its compressive strength f_{c}. Using the strength-stiffness relationships proposed by Model Code 2010 (CEB-FIP 2011), the degradation rate of the compressive and tensile strength of unaffected concrete shown to be lower than that for the elastic modulus (Figure 6(b)). To demonstrate this, ASR-affected concrete with a compressive strength reduction of 20% ($\beta_{f_{\mathrm{c}}} = 0.80$) is considered. Adopting the Model Code formulation, the estimated normalised values of the elastic modulus and tensile strength are 0.94 and 0.86, respectively. Considering the proposed curves, the degradation of the stiffness and tensile strength are substantially different; the normalised values are $\beta_E = 0.35$ and $\beta_{f_{\mathrm{t,sp}}} = 0.60$. This demonstrates that for ASR-affected concrete, the engineering strength-stiffness relationships cannot be used to determine the elastic modulus and the tensile strength from the measured compressive strength.

CONCLUDING REMARKS

The alkali-silica reaction is a harmful degradation process that can compromise the durability and serviceability of concrete structures. From investigations on structures and concrete members down to the microscopic level, numerous researchers have attempted to describe the structural consequences of ASR-induced concrete expansion with varying success. Although a literature survey shows that there is a strong coupling between concrete swelling and the degradation of mechanical properties, numerous findings have never led to a widely agreed upon picture. This paper attempted to clarify the relationship between concrete expansion due to the ASR and consequent degradation (or enhancement) of engineering properties.

First, the laboratory tests performed by the authors were presented. The authors investigated the evolution of the static elastic modulus, compressive strength and splitting tensile strength in two comparable reactive concrete mixes composed of Dutch and Norwegian aggregates. These tests belong to an extensive research project that aims to study the ASR degradation effects on various scales, from micro to macro, in order to better understand the phenomenon.

Second, available literature data, which focus on the evolution of engineering properties of ASR-affected concrete under free-expansion conditions, were collected and statistically analysed. When expressing the data as a function of the concrete expansion, a clear trend could be observed. The data were categorised into four reactivity classes: non-reactive ($\varepsilon < 0.05\%$), potentially reactive ($0.05\% \leq \varepsilon \leq 0.10\%$), reactive ($0.10\% < \varepsilon < 0.50\%$) and extremely reactive ($\varepsilon \geq 0.50\%$). A normalisation procedure was adopted: each normalised value was obtained as the ratio between the current value of the property and its (calculated) reference value, which corresponds to an expansion of 0.05%. The statistical analysis considered two fitting laws: an S-shaped curve and an piecewise linear curve.

The elastic modulus was identified as the best indicator of ASR signs in concrete, showing relevant degradation already at small expansion values. A deterioration of up to 90% could be observed. Both static and dynamic elastic modulus tests can contribute to the definition of the residual stiffness in the material. The curve fitting provides good results for both laws, with an estimation error of 7%.

The influence of the ASR on the compressive strength has been widely investigated. This test method is one of the principal techniques adopted in structural assessments. However, this method was determined to be the worst indicator in terms of monitoring the ASR. The compressive strength exhibits an initial gain of approximately 15% in the low- and moderate-expansion zones and a subsequent decreases to 46% of its original value. The piecewise linear curve provides the best fitting, thereby allowing the description of a non-monotonic trend. The estimation error is approximately 13%.

The splitting test best captured the influence of the ASR on the tensile behaviour of concrete. The data show an initial delay with respect to the degradation of the elastic modulus but a similar deterioration rate in the high-expansion zone. The splitting tensile strength eventually decreases to 64%. The S-shaped curve provided the best fitting with an estimation error of 8%.

When comparing the degradation behaviour of compressive and splitting tensile strengths with respect to the elastic modulus, a non-linear relation was observed. Consequently, the ASR-affected concrete appears to be a substantially different material and the known engineering strength-stiffness relationships, developed for unaffected concrete, cannot be applied.

The correlation between mechanical degradation and concrete expansion, which appears fundamental to the assessment of ASR-affected concrete structures, should be further investigated systematically to obtain narrowed bounds. Various parameters such as the specimen size, the storage conditions, the type of aggregates and the confinement of the samples, can play an important role in this phenomenon. To obtain statistically relevant data sets, additional experimental campaigns are necessary.

ACKNOWLEDGEMENTS

This work is part of the project ”Performance Assessment Tool for Alkali-Silica Reaction” (PAT-ASR, STW grant no. 10977, http://pat-asr.blogspot.nl/), which is developed in the context of the IS2C program (http://is2c.nl/). The authors wish to express their thanks to the Dutch National Foundation (STW), the Dutch Ministry of Infrastructures and the Environment (Rijkswaterstraat), SGS and TNO DIANA BV for their financial support. The authors are grateful to the Norwegian

Public Roads Administration (Statens Vegvesen) and SINTEF for their collaboration.

References

Ahmed, T., Burley, E., Rigden, S., and Abu-Tair, I. (2003). "The effect of alkali reactivity on the mechanical properties of concrete." *Construction and Building Materials*, 17(2), 123–144.

American Society for Testing and Materials (2001). *ASTM C1293 - Standard Test Method for Determination of Length Change of Concrete Due to Alkali-Silica Reaction*. West Conshohocken, PA, United States.

American Society for Testing and Materials (2012a). *ASTM C127 - Standard Test Method for Density, Relative Density (Specific Gravity), and Absorption of Coarse Aggregate*. West Conshohocken, PA, United States.

American Society for Testing and Materials (2012b). *ASTM C128 - Standard Test Method for Density, Relative Density (Specific Gravity), and Absorption of Fine Aggregate*. West Conshohocken, PA, United States.

Anaç, C., Esposito, R., Çopuroğlu, O., Schlangen, E., and Hendriks, M. (2012). "A tool for concrete performance assessment for ASR affected structures: an outlook." *14th International Conference on Alkali Aggregate Reaction (ICAAR14)*, Austin, Texas.

Bažant, Z., Zi, G., and Meyer, C. (2000). "Fracture mechanics of ASR in concretes with waste glass particles of different sizes." *ASCE Journal of Engineering Mechanics*, 126(3), 226–232.

Ben Haha, M. (2006). "Mechanical effects of alkali silica reaction in concrete studied by SEM-image analysis." Ph.D. thesis, Èncole Polytechnique Fèdèrale de Lusanne, Lusanne, Switzerland (May).

Capra, B. and Sellier, A. (2003). "Orthotropic modelling of alkali-aggregate reaction in concrete structures: numerical simulations." *Mechanics of Materials*, 35(8), 817–830.

CEB-FIP (2011). *Model Code for Concrete Structures (MC2010)*. International Federation for Structural Concrete (fib), Lausanne, Switzerland.

Clayton, N., Currie, R., and Moss, R. (1990). "The effects of alkali-silica reaction on the strength of prestressed concrete beams." *The Structural Engineer*, 68(15), 287–292.

Comi, C., Fedele, R., and Perego, U. (2009). "A chemo-thermo-damage model for the analysis of concrete dams affected by alkali-silica reaction." *Mechanics of Materials*, 41(3), 210–230.

den Uijl, J. (2002). "Structural consequences of ASR: an example on shear capacity." *Heron*, 47(2), 125–139.

Fan, S. and Hanson, J. (1998). "Effect of alkali silica reaction expansion and cracking on structural behavior of reinforced concrete beams." *ACI Structural Journal*, 95, 498–505.

Giaccio, G., Zerbino, R., Ponce, J., and Batic, O. (2008). "Mechanical behavior of concretes damaged by alkali-silica reaction." *Cement and Concrete Research*, 38(7), 993–1004.

Giannini, E. and Folliard, K. (2012). "Stiffness damage and mechanical testing of cores specimens for the evaluation of structures affected by ASR." *14th International Conference on Alkali Aggregate Reaction (ICAAR14)*, Austin, Texas.

Huang, M. and Pietruszczak, S. (1999). "Modeling of thermomechanical effects of alkali-silica reaction." *Journal of Engineering Mechanics*, 125(4), 476–485.

Inoue, A., Mikata, Y., Takahashi, Y., and Inamasu, K. (2012). "Residual shear capacity of ASR damaged reinforced concrete beams with ruptured stirrups." *14th International Conference on Alkali Aggregate Reaction (ICAAR14)*, Austin, Texas.

International Organization for Standardization (2010). *ISO 1920-10:2010(E) Testing of concrete - Part 10: Determination of static modulus of elasticity in compression*. Geneva, Switzerland.

Larive, C. (1998). "Apports combinès de l expèrimentation et de la modèlesllisation á la comprehènsion de l'alcali-rèaction et de ses effets mècaniques." Ph.D. thesis, Èncole Nationale des Ponts et Chaussèes, Èncole Nationale des Ponts et Chaussèes.

Léger, P., Côté, P., and Tinawi, R. (1996). "Finite element analysis of concrete swelling due to alkali-aggregate reactions in dams." *Computers & Structures*, 60(4), 601–611.

Li, K. and Coussy, O. (2004). "Numerical assessment and prediction method for the chemico-mechanical deterioration of ASR-affected concrete structures." *Canadian Journal of Civil Engineering*, 31(3), 432–439.

Lindgård, J. (2013). "Alkali-silica reaction (ASR) - performance testing." Ph.D. thesis, Norwegian University of Science and Technology, Norwegian University of Science and Technology (October).

Malla, S. and Wieland, M. (1999). "Analysis of an arch-gravity dam with a horizontal crack." *Computers & Structures*, 72, 267–278.

Martin, R., Renaud, J., Multon, S., Toutlemonde, F., et al. (2012). "Structural behavior of plain and reinforced concrete beams affected by combined AAR and DEF." *14th International Conference on Alkali Aggregate Reaction (ICAAR14)*, Austin, Texas.

Mikata, Y., Shimazu, Y., Hatano, Y., and Inoue, S. (2012). "Flexural and shear capacity of prc beams damaged by combined deterioration due to asr and corrosion." *14th International Conference on Alkali Aggregate Reaction (ICAAR14)*, Austin, Texas.

Miyagawa, T., Yokoyama, T., Yonekawa, H., Mita, T., Nakamura, K., and Ookubo, T. (2012). "Strengthening effect on prestressed concrete memebrs affected by alkali-silica reaction (ASR)." *14th International Conference on Alkali Aggregate Reaction (ICAAR14)*, Austin, Texas.

Monette, L. J. (1997). "Effects of the alkali-silica reaction on unloaded, statically loaded and dynamically loaded reinforced concrete beams." M.S. thesis, University of Ottawa, Ottawa, Ontario, Canada.

Multon, S. (2004). "Evaluation expèrimental et thèorique des effets mècaniques de l'alcali-rèaction sur des structures modéles." Ph.D. thesis, Universitè de Marne-la-Vallèe (in collaboration with LCPC-EDF), Champs sur Marne (October).

Nederlands Normalisatie-instituut (2002). *NEN-EN 12390-3 Testing hardened concrete - Part 3: Compressive strength of test specimens*. Delft, The Netherlands.

Nederlands Normalisatie-instituut (2009). *NEN-EN 12390-6 Testing hardened concrete - Part 6: Tensile splitting strength of test specimens*. Delft, The Netherlands.

Ramezanianpour, A. and Hajighasemali, S. (2012). "Flexural strength of ASR affected beams under sustained loading." *14th International Conference on Alkali Aggregate Reaction (ICAAR14)*, Austin, Texas.

RILEM TC 219-ACS Alkali-Silica Reaction in Concrete Structures (2011). *RILEM Recommended*

Test Method: AAR-3 - Detection of potential alkali-reactivity - 38^{o}C test method for aggregate combinations using concrete prisms (Final draft) (September).

RILEM TC 219-ACS Alkali-Silica Reaction in Concrete Structures (2012). *RILEM Recommended Test Method: AAR-0 - Outline Guide to the Use of RILEM Methods in the Assessment of the Alkali-Reactivity Potential of Aggregates (Final draft)* (May).

Sanchez, L., Fournier, B., Jolin, M., and Bastien, J. (2014). "Evaluation of the stiffness damage test (SDT) as a tool for assessing damage in concrete due to ASR: Test loading and output responses for concretes incorporating fine or coarse reactive aggregates." *Cement and Concrete Research*, 56, 213–229.

Saouma, V. (2013). *Numerical Modeling of AAR*. CRC Press.

Saouma, V. and Perotti, L. (2006). "Constitutive model for alkali-aggregate reactions." *ACI Materials Journal*, 103(3), 194–202.

Saouma, V., Perotti, L., and Shimpo, T. (2007). "Stress, analysis of concrete structures subjected to alkali-aggregate, reactions." *ACI Structural Journal*, 104(5), 532–541.

Sargolzahi, M., Kodjo, S., Rivard, P., and Rhazi, J. (2010). "Effectiveness of nondestructive testing for the evaluation of alkali-silica reaction in concrete." *Construction and Building Materials*, 24(8), 1398–1403.

Swamy, R. and Al-Asali, M. (1988). "Engineering properties of concrete affected by alkali-silica reaction." *ACI Materials Journal*, 85(5), 367–374.

Ulm, F.-J., Coussy, O., Li, K., and Larive, C. (2000). "Thermo-chemo-mechanics of ASR expansion in concrete structures." *ASCE Journal of Engineering Mechanics*, 126(3), 233–242.

List of Tables

Table 1: Mixture proportions.

Material	Amount $\mathrm{kg/m^3}$	Density $\mathrm{kg/m^3}$	ASG $\mathrm{m^2/kg}$	Absorption %	Moisture w.%
RR1 mix (natural Dutch aggregates)					
Cement	380	3160			
Water	175				
Aggregate 0-2 mm	581	2551	5.36	0.77	0.26
Aggregate 2-4 mm	269	2551	1.95	0.77	0.26
Aggregate 4-8 mm	264	2582	0.52	0.41	0.07
Aggregate 8-16 mm	443	2598	0.31	0.23	0.04
Aggregate 16-22 mm	195	2599	0.23	0.49	0.27
RR2 mix (crushed Norwegian aggregates)					
Cement	380	3160			
Water	171				
Aggregate 0-2 mm	601	2651	5.36	0.28	0.03
Aggregate 2-4 mm	278	2651	1.95	0.28	0.03
Aggregate 4-8 mm	273	2691	0.52	0.28	0.07
Aggregate 8-16 mm	460	2718	0.31	0.12	0.06
Aggregate 16-22 mm	200	2688	0.23	0.17	0.07

Table 2: Physical and chemical characteristics of the cement.

Property	Value	Unit
Physical properties (cf. EN 196)		
Particle analysis +90 μm	0	%
Particle analysis +64 μm	0	%
Particle analysis -24 μm	88.6	%
Particle analysis -30 μm	94.3	%
Specific surface, Blaine	565	m^2/kg
Compressive strength at 1 d	29.7	MPa
Compressive strength at 2 d	39.0	MPa
Compressive strength at 7 d	47.9	MPa
Compressive strength at 28 d	57.0	MPa
Chemical properties (cf. EN 196-2)		
Loss on ignition (L.O.I.)	2.21	%
Free lime	2.08	%
Tot. Chloride	0.05	%
Sulphur Trioxide SO_3	3.34	%
Silica SiO_2	19.88	%
Alumina Al_2O_3	4.85	%
Ferric Oxide Fe_2O_3	3.76	%
Lime CaO	61.71	%
Magnesia MgO	2.43	%
Phosphorus Pentoxide P_2O_5	0.15	%
Potassium Oxide K_2O	1.02	%
Sodium Oxide Na_2	0.50	%
Alkali Na_2O_{eq}	1.17	%

Table 3: Concrete properties for each cast.

Property	Unit	Value					
Cast		1	2	3	4	5	6
Mix		RR1	RR1	RR2	RR1	RR2	RR2
Specific weight	$\mathrm{kg/m^3}$	2340	2386	2389	2382	2450	2434
Air content	%	4.8	2.7	3.6	2.4	3.3	3.8
Slump H	mm	100	-	90	215	165	120
Slump d	mm	345	565	355	427.5	462.5	407.5
28-d compressive strength	MPa	60.40	67.95	62.44	62.14	68.10	61.80

Table 4: Storage conditions of RR1 and RR2 concrete samples.

Test		Unit	Expansion	Static elastic modulus Compressive strength Poisson ratio	Splitting tensile strength	Control casting
Sample size		mm	75x75x280	100x100x400	150x150x150	150x150x150
No. samples			6	42	42	18
After casting	Time	d	1	1	1	1
	Temp.	^oC	20	20	20	20
	RH	%	98	98	98	98
Pre-treatm.	Time	d	No pre-treatment	No pre-treatment	No pre-treatment	28
	Temp.	^oC				20
	RH	%				98
ASR treatm.	Time	d	365	various up to 365	various up to 365	No ASR treatment
	Temp.	^oC	38	38	38	
	RH	%	96	96	96	
Before test	Time	h	24	> 2	> 2	> 2
	Temp.	^oC	20	20	20	20
	RH	%	50	50	50	50

Table 5: Experimental results and calculated reference values for normalisation procedure.

	RR1						RR2					
Time d	Cast	ε %	E_{st} GPa	ν	f_{c} MPa	$f_{\mathrm{t,sp}}$ MPa	Cast	ε %	E_{st} GPa	ν	f_{c} MPa	$f_{\mathrm{t,sp}}$ MPa
14	4 - 4	-0.002	42.1	0.19	45.7	3.95	5 - 5	0.001	29.2	0.20	53.7	4.45
28	4 - 1	0.002	42.7	0.20	50.6	3.90	5 - 3	0.004	30.5	0.21	58.5	4.30
49	4 - 1	0.005	43.1	0.26	54.3	4.30	5 - 3	0.011	33.0	0.29	59.7	4.20
91	4 - 1	0.009	43.1	0.20	53.7	4.40	5 - 3	0.018	27.4	0.24	63.7	4.55
182	4 - 2	0.037	38.9	0.28	59.4	3.85	5 - 6	0.067	25.5	0.25	60.0	3.50
252	4 - 2	0.079	40.7	0.18	61.8	3.60	5 - 6	0.123	17.0	0.27	60.1	3.50
364	4 - 2	0.113	40.1	0.18	63.0	3.30	5 - 6	0.179	17.4	0.25	59.5	3.30
Calc. ref. value		0.05	39.5	0.24	60.11	3.76		0.05	26.1	0.25	61.23	3.85

Table 6: Overview of experimental tests in the literature: concrete properties.

Author	Data set	Aggregate Type	Cement	W/C	Na2Oeq %
Swamy	ER1	amorphous fused silica (fine)	520	0.44	1.00
	ER2	Beltane opal (fine)			
Larive	RR	Tournaisis limestone (fine and coarse)	410	0.44	1.25
Monette	RR	siliceous limestone (fine and coarse)	423	0.61	1.25
Ahmed	RR	limestone (fine and coarse)	400	0.50	1.75
	ER1	Thames Valley sand (fine) and limestone (coarse)			
	ER2	Thames Valley sand (fine), fused silica (fine) and limestone (coarse)			
Multon	PR	calcareous stones with siliceous inclusions	410	0.50	1.25
Ben Haha	PR1ia-b	chlorite interleaved	-	0.46	0.40
	PR1iia-b-c	with layers of quartz and feldspar			0.80
	PR1iiia-b-c	(fine and coarse)			1.20
	PR2ia-b	biotitic schist			0.40
	PR2iia-b-c	containing phyllosilicates			0.80
	PR2iiia-b-c	(fine and coarse)			1.20
Giaccio	PR	granitic stone with feldspars, quartz, micas, epidote, zircon	420	0.42	1.24
	RR1	siliceous orthoquartzite with opal, quartz, chalcedony, microcrystalline			
	RR2	opal, chalcedony			
Sargolzahi	RR	Spratt limestone	345	0.50	1.25
Giannini	RR1	rhyolite and other volcanics (coarse)	420	0.42	1.25
	RR2	quartz, feldspars, siliceous volcanics, chert (fine)			
Lindgård	PR1a		400	0.45	2.25
	PR2a		550	0.30	0.67
	RR1a		315	0.60	1.17
	RR2a	Ottersbo	400	0.45	0.93
	PR1b	cataclasite	400	0.45	2.25
	PR2b	with crypto-	550	0.30	0.67
	RR1b	to microcystalline	315	0.60	1.17
	RR2b	quartz	400	0.45	0.93
	PR1c	(coarse)	400	0.45	2.25
	PR2c		550	0.30	0.67
	RR1c		315	0.60	1.17
	RR2c		400	0.45	0.93
Sanchez	RR1i	mixed	314	0.61	1.25
	RR1ii	volcanics and	370	0.47	
	RR1iii	chert (fine)	424	0.37	
	RR2i	mixed	314	0.61	
	RR2ii	volcanics and	370	0.77	
	RR2iii	chert (coarse)	424	0.37	
Esposito	RR1	quartzite, quartz, (calcareous) chert, volcanic rock fragments (fine and coarse)	380	0.45	1.17
	RR2	coarse grained quartz, quartzite, gneiss, metarhyolite (fine and coarse)			

Table 7: Overview of experimental tests in the literature: storage conditions.

Author		Pre-treatment				ASR development			
		Time d	Wrap.	Temp. °C	Moist.	Time d	Wrap.	Temp. °C	Moist.
Swamy		No	No	No	No	365	No	20	96%
Larive		11	Al-foil	23	98%	546	No	38	97%
Monette		28	No	20	96%	147	No	38	1N NaOH solution
Ahmed		28	No	20	in water	365	No	38	in water
Multon		28	Al-foil	20	N/A	730	Al-foil	38	in box
Ben Haha	a	No	No	No	No	365	No	20	in box on water
	b							40	
	c							60	
Giaccio		No	No	No	No	721/904	cotton	38	plastic bag with 5 ml water
Sargolzahi		7	No	20	97%	700	No	38	in plastic box on water
Giannini		No	No	No	No	120/270	No	38	95%
Lindgård	a	1/7/28	No	20	96%	365/784	No	38	in plastic box
	b				in water (0.5hrs)	273	cotton	60	in metal box on water
	c				in water (0.5hrs)	365/273	cotton	38	in plastic box with lining
Sanchez		No	No	No	No	63/182	No	38	100%
Esposito		No	No	No	No	365	No	38	96%

Table 8: Overview of experimental tests in the literature: data name and corresponding marker in figures, asymptotic expansion and calculated reference values of the measured mechanical properties.

Author	Data set#		Expansion		Calculated reference value at ε = 0.05%					
			Time	ε	E_{st}	E_{dyn}	f_{c}	$f_{\mathrm{t,sp}}$	MOR	$f_{\mathrm{t,dir}}$
			d		GPa	GPa	MPa	MPa	MPa	MPa
Swamy	ER1	+	365	0.62	-	39.0	52.53	3.24	4.08	-
	ER2	×	365	1.64	-	34.3	43.08	-	-	-
Larive	RR	∗	365	0.21”	33.9	-	52.64	3.93	-	-
Monette	RR	×	147	0.35	18.8	38.2	27.51	-	5.87	-
Ahmed	RR	□ w	365	0.15	32.7	-	51.15	4.74	5.37	4.80
	ER1	□ g	365	0.73	36.3	-	50.30	5.05	6.76	2.60
	ER2	□ b	365	2.70	22.1†	-	41.22†	3.57†	5.26†	1.42†
Multon	PR	+	365	0.10	32.6	-	42.01	3.14	-	-
Ben Haha	PR1ia	▽w	365	0.05	24.8	-	63.86	4.35	-	-
	PR1iia	▽g	365	0.07	24.8	-	51.43	3.81	-	-
	PR1iiia	▽b	365	0.08	25.2	-	53.62	4.05	-	-
	PR1ib‡	△w	365	0.05	21.8	-	51.09	4.39	-	-
	PR1iib‡	△g	365	0.12	26.8	-	48.27	4.27	-	-
	PR1iiib‡	△b	365	0.14	25.0	-	46.15	4.25	-	-
	PR1iic	◇g	365	0.14	25.0	-	46.15	4.25	-	-
	PR1iiic	◇b	365	0.16	26.5	-	47.53	4.36	-	-
	PR2ia	▽w	365	0.05	26.4	-	34.26	4.25	-	-
	PR2iia	▽g	365	0.07	25.7	-	55.72	3.81	-	-
	PR2iiia	▽b	365	0.07	24.9	-	54.73	3.93	-	-
	PR2ib‡	△w	365	0.12	26.7	-	50.47	4.22	-	-
	PR2iib‡	△g	365	0.14	26.0	-	48.98	4.33	-	-
	PR2iiib‡	△b	365	0.14	25.8	-	47.93	4.25	-	-
	PR2iic	◇g	365	0.14	25.5	-	49.21	4.37	-	-
	PR2iiic	◇b	365	0.16	26.2	-	47.47	4.37	-	-
Giaccio	PR	∘w	365	0.08	38.1	-	36.50	-	-	-
	RR1	∘g	365	0.21	24.1†	-	30.20†	-	-	-
	RR2	∘b	365	0.28	32.0	-	27.80	-	-	-
Sargolzahi	PR	*	365	0.08”	32.5	20.9	43.02	-	-	-
Giannini	RR1	□ w	120	0.14	25.5	-	36.82	-	-	-
	RR2	□ b	270	0.42	25.4	-	34.52	-	-	-
Lindgård	PR1a‡	◁g	365	0.05	-	44.7	-	-	-	-
	PR2a‡	◁w	365	0.08	-	51.6	-	-	-	-
	RR1a‡	▷g	365	0.21	-	36.5	-	-	-	-
	RR2a‡	▷w	365	0.26	-	42.1	-	-	-	-
	PR1b	◁g	273	0.14	-	43.2	-	-	-	-
	PR2b	◁w	273	0.17	-	47.6	-	-	-	-
	RR1b	▷g	273	0.18	-	34.7	-	-	-	-
	RR2b	▷w	273	0.23	-	38.7	-	-	-	-
	PR1c	◁g	273	0.04	-	40.3†	-	-	-	-
	PR2c	◁w	273	0.06	-	49.1	-	-	-	-
	RR1c	▷g	273	0.28	-	37.8	-	-	-	-
	RR2c	▷w	365	0.27	-	42.7	-	-	-	-
Sanchez	RR1i	∘w	63	0.30	-	21.0	-	-	-	-
	RR1ii	∘g	63	0.30	-	29.5	-	-	-	-
	RR1iii	∘b	63	0.30	-	28.0	-	-	-	-
	RR2i	∘w	182	0.20	-	23.2	-	-	-	-
	RR2ii	∘g	182	0.20	-	30.9	-	-	-	-
	RR2iii	∘b	182	0.20	-	29.3	-	-	-	-
Esposito	RR1	⋆b	365	0.11	39.5	-	60.11	3.76	-	-
	RR2	⋆g	365	0.18	26.1	-	61.23	3.85	-	-

‡ Sample used for the classification (for authors who tested the same mix in different storage conditions).
” Interpolated expansion value.
† Extrapolated value of the mechanical properties at the reference expansion. All the other data are interpolated.
# Data set and adopted marker in figures. If the symbol is repeated the size is decreased (e.g. Swamy-ER1 is identified with a larger + sign with respect to Multon-PR). The filler of the markers can be white (w), grey (g) or black (b).

Table 9: Fitting coefficients and standard deviation.

Data	S-curve					Piecewise linear curve					
	ε_c %	ε_l %	β_0	β_∞	σ %	q_l	m_l	m_m	m_h	m_e	σ %
E	0.37	$1.13\ 10^{-9}$	1.06	0.19	7	1.07	-1.06	-1.78	-0.98	-0.23	7
E_st	0.42	$2.27\ 10^{-14}$	1.05	0.11	9	1.04	-0.46	-1.89	-1.08	-0.21	9
E_dyn	0.31	$6.89\ 10^{-12}$	1.07	0.29	6	1.08	-1.43	-1.75	-0.91	-0.26	6
f_c	0.07	1.13	1.00	0.64	15	0.89	2.36	2.06	-0.37	-0.18	13
f_t	$5.24\ 10^{-04}$	0.51	1.00	0.59	15	1.01	-0.15	0.20	-0.83	-0.08	15
$f_\mathrm{t,sp}$	0.11	0.35	1.01	0.60	8	1.01	-0.25	-0.15	-0.86	-0.04	8
MOR	0.07	0.37	1.05	0.34	20	1.06	0.53	0.04	-1.54	-0.14	20
$f_\mathrm{t,dir}$	0.10	2.15	1.05	0.70	12	0.97	2.23	-0.68	0.20	-0.18	13

List of Figures

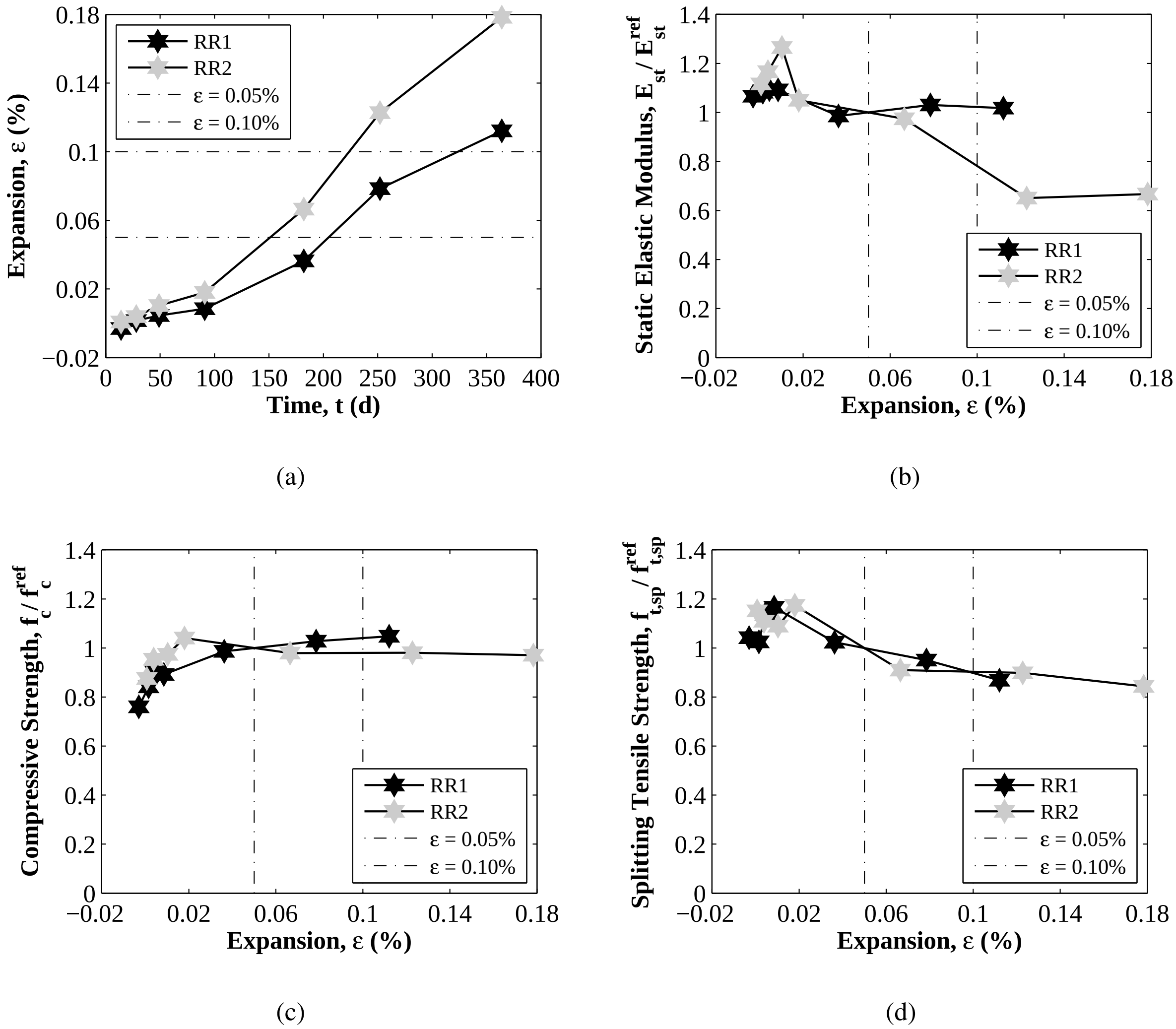

Figure 1: Expansion behaviour (a) and deterioration of static elastic modulus (b), compressive strength (c) and splitting tensile strength (d) for the RR1 and RR2 concrete mixes.

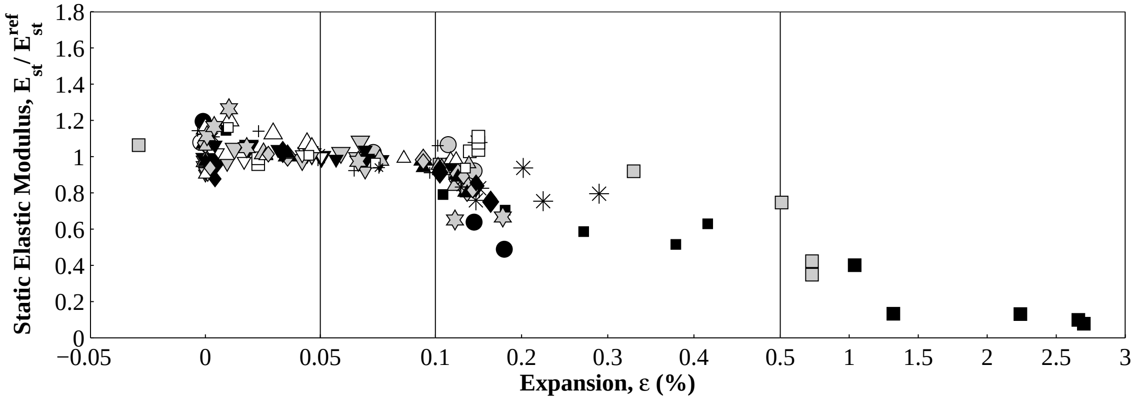

(a)

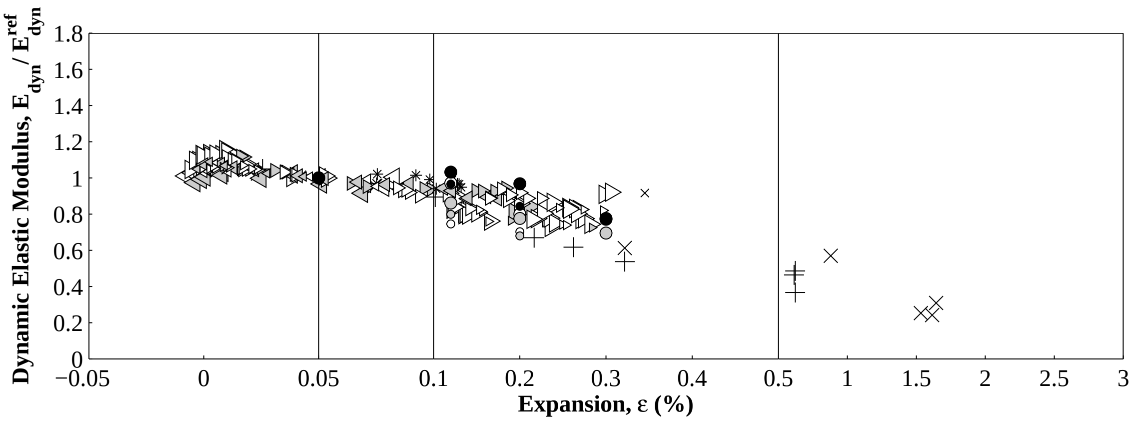

(b)

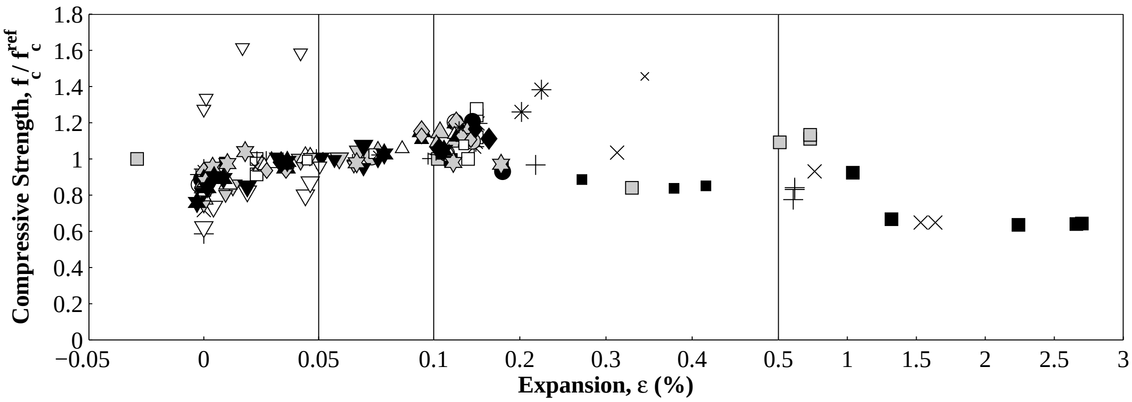

(c)

Figure 2: Experimental data from the literature: (a) Static elastic modulus; (b) Dynamic elastic modulus; (c) Compressive strength. A non-uniform scale for the expansion axis is used. For the legend see the description in Table 8.

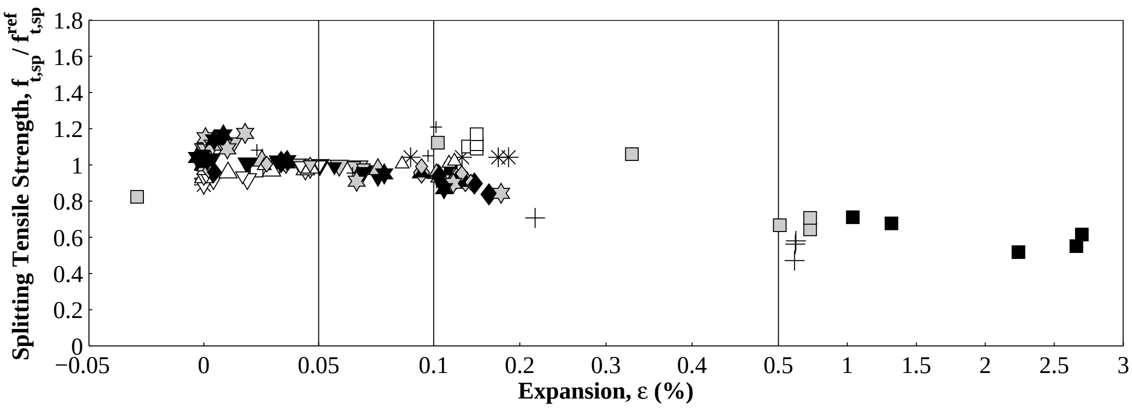

(a)

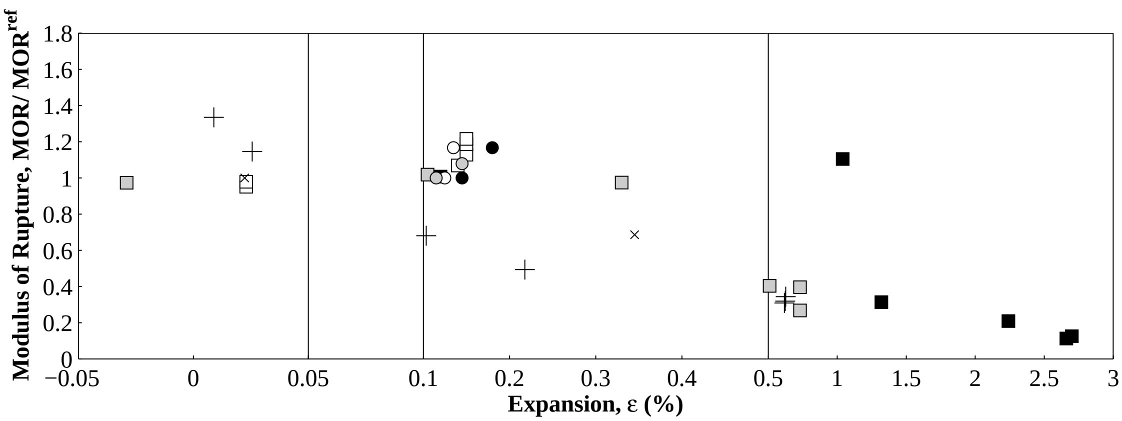

(b)

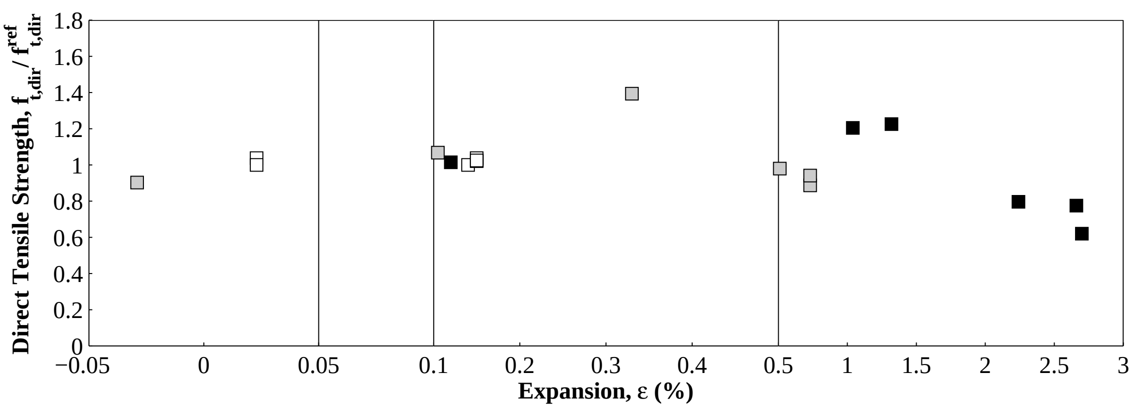

(c)

Figure 3: Experimental data from literature: (a) Splitting tensile strength; (b) Modulus of rupture; (c) Direct tensile strength. A non-uniform scale for the expansion axis is used. For the legend see the description in Table 8.

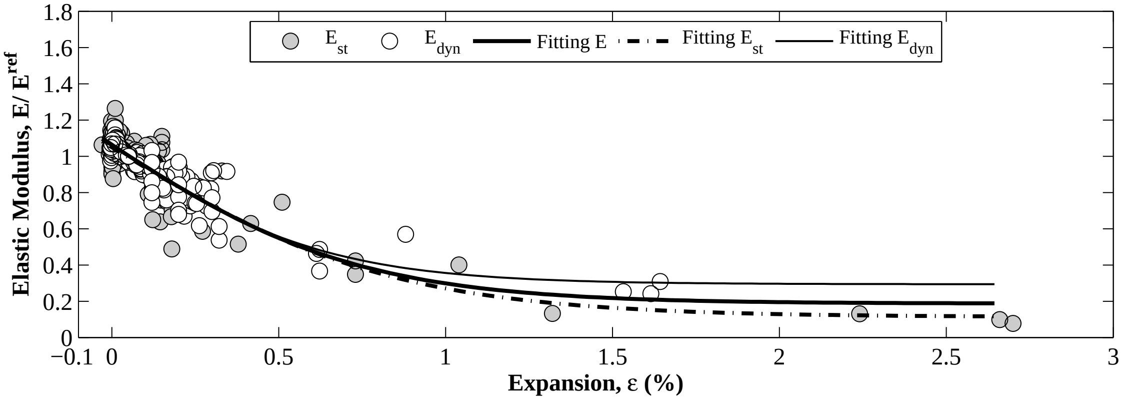

(a)

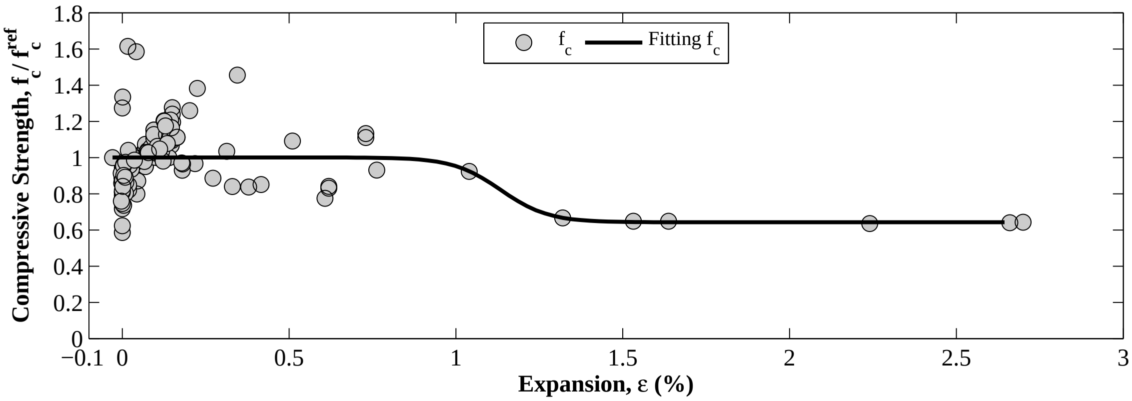

(b)

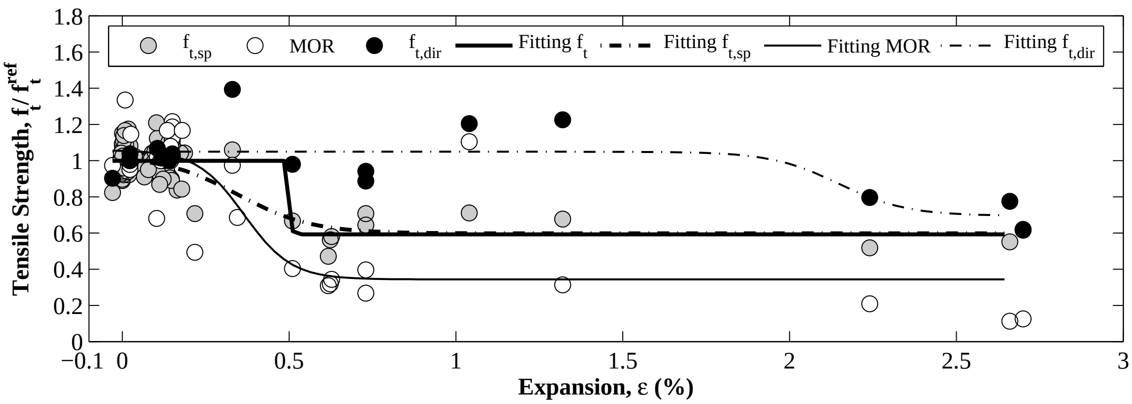

(c)

Figure 4: Fitting adopting S-shaped curve: (a) Elastic modulus; (b) Compressive strength; (c) Tensile strength.

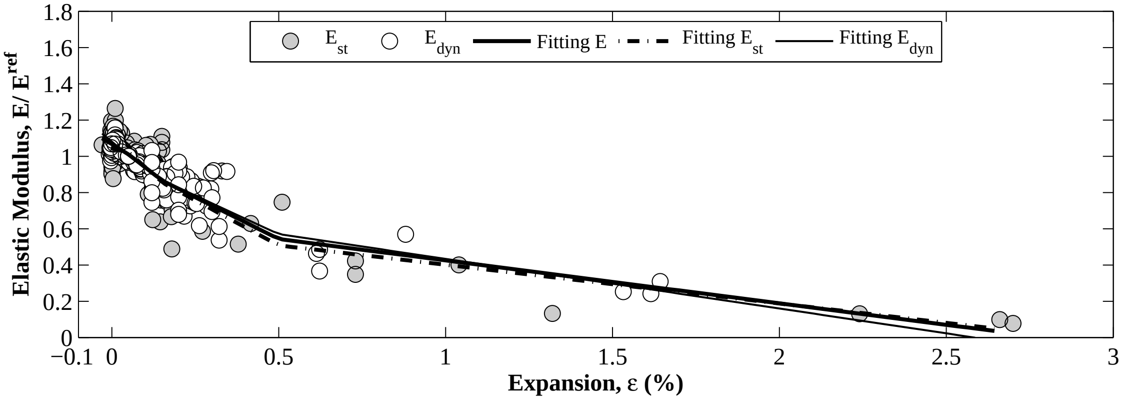

(a)

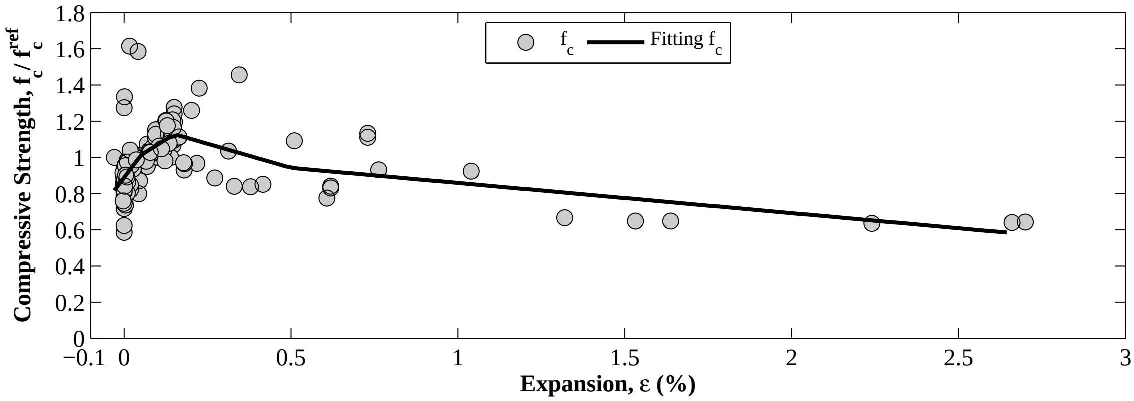

(b)

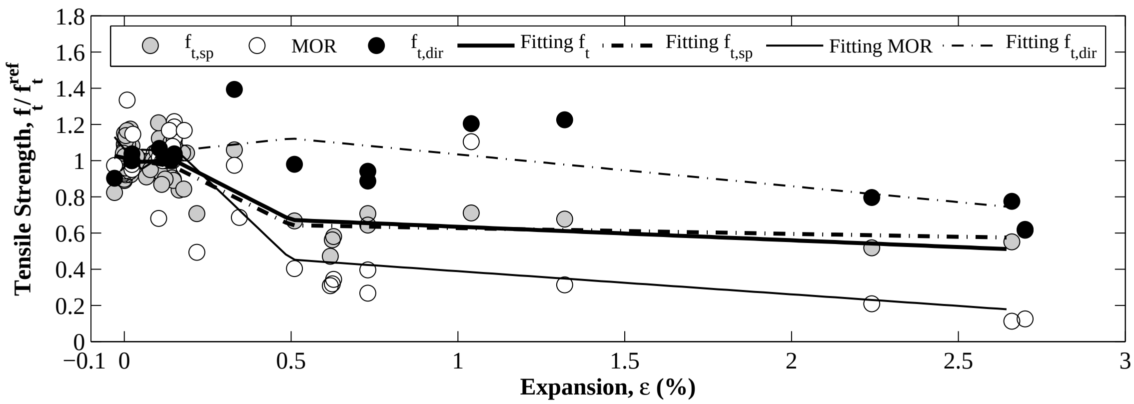

(c)

Figure 5: Fitting adopting piecewise linear curve: (a) Elastic modulus; (b) Compressive strength; (c) Tensile strength.

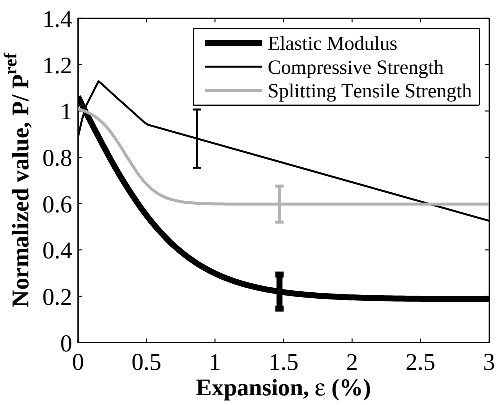

(a)

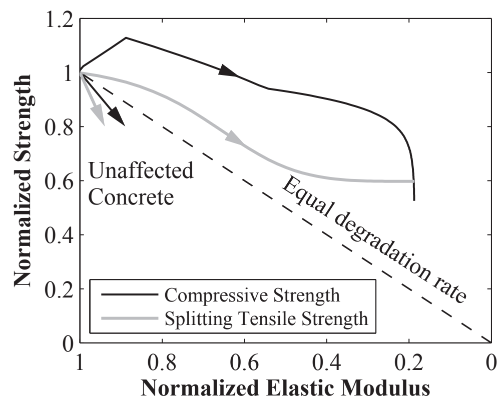

(b)

Figure 6: Best curve fitting results: (a) Relation between normalised properties and concrete expansion; (b) Relation between normalised elastic modulus and normalised strengths.